

EMO-X: Efficient Multi-Person Pose and Shape Estimation in One-Stage

Haohang Jian^{1*} Jinlu Zhang^{2*} Junyi Wu³ Zhigang Tu^{1†}

¹Wuhan University

²Center on Frontiers of Computing Studies, School of Computer Science, Peking University

³Fuzhou University

Abstract

*Expressive Human Pose and Shape Estimation (EHPS) aims to jointly estimate human pose, hand gesture, and facial expression from monocular images. Existing methods predominantly rely on Transformer-based architectures, which suffer from quadratic complexity in self-attention, leading to substantial computational overhead, especially in multi-person scenarios. Recently, Mamba has emerged as a promising alternative to Transformers due to its efficient global modeling capability. However, it remains limited in capturing fine-grained local dependencies, which are essential for precise EHPS. To address these issues, we propose **EMO-X**, the **Efficient Multi-person One-stage** model for multi-person EHPS. Specifically, we explore a Scan-based Global-Local Decoder (SGLD) that integrates global context with skeleton-aware local features to iteratively enhance human tokens. Our EMO-X leverages the superior global modeling capability of Mamba and designs a local bidirectional scan mechanism for skeleton-aware local refinement. Comprehensive experiments demonstrate that EMO-X strikes an excellent balance between efficiency and accuracy. Notably, it achieves a significant reduction in computational complexity, requiring **69.8%** less inference time compared to state-of-the-art (SOTA) methods, while outperforming most of them in accuracy.*

1. Introduction

Expressive Human Pose and Shape Estimation (EHPS) plays a crucial role in applications such as virtual reality and human-computer interaction, obtaining increasing attention in recent years. Its objective is to jointly estimate human body pose, hand gesture, and facial expression from monocular images, which plays an important role in human behavior understanding, motion capture, human-computer interaction, gaming industries, etc. This task typically em-

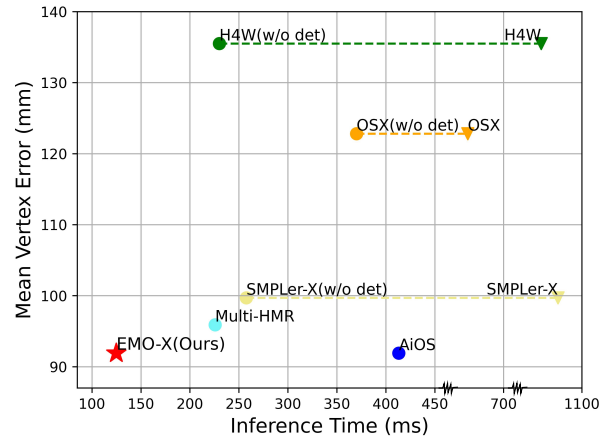


Figure 1. Comparison of estimation error and inference time across recent advanced EHPS methods on the AGORA dataset. The number of individuals in the test case is set to 5. For multi-stage methods, we report the inference time with and without the detector separately. The proposed EMO-X attains superior performance on both accuracy and efficiency.

plloys parametric human models (e.g., SMPL-X [1]) to represent highly complicated human body, face, and hands.

Building upon the success of single-part pose and shape estimation [2–10, 12], existing methods [13–16, 18] usually use a multi-stage pipeline. Where these methods typically first detect and crop regions corresponding to the body, face, and hands, subsequently feeding these isolated parts into separate expert networks for parameter estimation. However, this pipeline is in a complex multi-stage style and separates information between different components, leading to inconsistent and unnatural articulation of the mesh and implausible 3D wrist rotations, especially in challenging scenarios involving occlusions or truncations. Therefore, some methods [17, 19] no longer crop specific parts separately, but perform holistic regression. However, they still rely on cropping individual persons from the image, making their performance highly sensitive to the quality of the bounding boxes from pre-trained detectors [57, 58]. Fur-

*Haohang Jian and Jinlu Zhang contributed equally to this work.

†Zhigang Tu is the corresponding author (tuzhigang@whu.edu.cn).

thermore, the contextual information regarding the relative positions is lost during this cropping process.

To handle these limitations, several one-stage methods [20–24] have been presented, which directly regress multi-person pose and shape parameters from the entire image. Multi-HMR [23] first predicts the human center heatmap, then regresses parameters by applying self-attention and cross-attention to the corresponding tokens within the prediction head. AiOS [24] adopts a DETR [25] style architecture, representing each person as a collection of box tokens and joint tokens. Similarly, by leveraging self-attention and cross-attention mechanisms, AiOS enriches feature representations before regressing the parameters, achieving impressive accuracy. Due to the ability to capture long-range dependency, these transformer-based architectures [26] have demonstrated remarkable success in EHPS. However, the quadratic complexity of self-attention calculations leads to a significant increase in computation demands as the number of tokens grows, especially in multi-person estimation scenarios. Which results in low inference efficiency, posing challenges for deployment on devices with limited computational resources.

Recently, with the development of State Space Models (SSMs), like Mamba [27], numerous models [28, 29] have been proposed for various vision tasks. The Mamba architecture is attractive due to its linear computational complexity and excellent long-range dependency modeling ability. However, the standard Mamba lacks the capacity to model local dependency, which is not conducive to refine highly structured human features.

To address these issues, we propose EMO-X, a novel efficient one-stage model for multi-person EHPS. Inspired by DETR-style methods [24, 44, 51] and Mamba-based approaches applied in vision tasks [28, 29], we represent human queries as learnable content queries and location queries, and introduce a Scan-based Global-Local Decoder (SGLD) to gradually refine them and finally regress whole-body parameters. We leverage the Mamba architecture’s excellent capability for modeling long-range dependencies to model the global space while introducing a novel Local Bidirectional Scan mechanism for skeleton-aware local refinement. Our approach maintains efficiency while ensuring the effective utilization of global and local features. Extensive experiments on multiple datasets [1, 19, 33, 34] demonstrate the superior accuracy and efficiency of our approach, as shown in Fig. 1. Remarkably, the proposed EMO-X reduces the inference time by 69.8% compared to state-of-the-art methods, and achieves higher accuracy than most of the existing approaches. This is crucial for real-time multi-person EHPS.

Our contributions can be summarized as follows:

- We propose a novel one-stage method, EMO-X, for multi-person Expressive Human Pose and Shape esti-

mation (EHPS). It combines the efficient and qualitative long-range modeling capability of Mamba meanwhile considering local details based on human skeleton.

- We exploit an efficient Scan-based Global-Local Decoder (SGLD) to progressively refine human tokens, which comprehensively considers global context and local details, and exploit a novel Local Bidirectional Scan mechanism for local skeleton-aware refinement.
- Extensive experiments on multiple benchmarks demonstrate that our EMO-X has fewer parameters and computational complexity while maintaining satisfactory accuracy. Compared with state-of-the-art (SOTA) methods, EMO-X reduces **69.8%** inference time.

2. Related Work

2.1. Expressive Human Pose and Shape Estimation

EHPS aims to jointly estimate human body poses, hand gestures, and facial expressions from monocular images and recover whole-body meshes. Based on the development of parametric models [1, 30–32], meshes can be directly obtained by regressing the model parameters. Early studies [13–16, 18] adopted a multi-stage pipeline, which required additional cropping and processing of hands and faces, and fed them to separate expert networks for parameter regression. ExPose [15] introduces body-driven attention for face and hand regions in the original image to extract higher-resolution crops that are fed to dedicated refinement modules. PIXIE [13] introduces a novel moderator that merges the features of the different experts adaptively. However, this complex multi-stage pipeline and information separation between different components leads to inconsistent and unnatural articulation of the mesh and implausible 3D wrist rotations, especially in challenging scenarios involving occlusions or truncations.

With the introduction of more full-body datasets [19, 33–37], holistic whole-body regression has become the prevailing approach [17, 19, 23, 24]. For single-person EHPS, OSX [19] proposes the first one-stage pipeline based on a designed Component-Aware Transformer. SMPLer-X [17] further amplifies one-stage methods by exploring both data and model scaling. However, for multi-person EHPS, these methods still require cropping each individual in the image, making performance highly dependent on bounding box quality and leading to the loss of valuable relative positional information. To address this, Multi-HMR [23] first predicts the human center heatmap, then regresses the parameters by applying the attention mechanism to the corresponding tokens within the prediction head. AiOS [24] adopts a DETR [25] style architecture, representing each person as a collection of box tokens and joint tokens. The self-attention

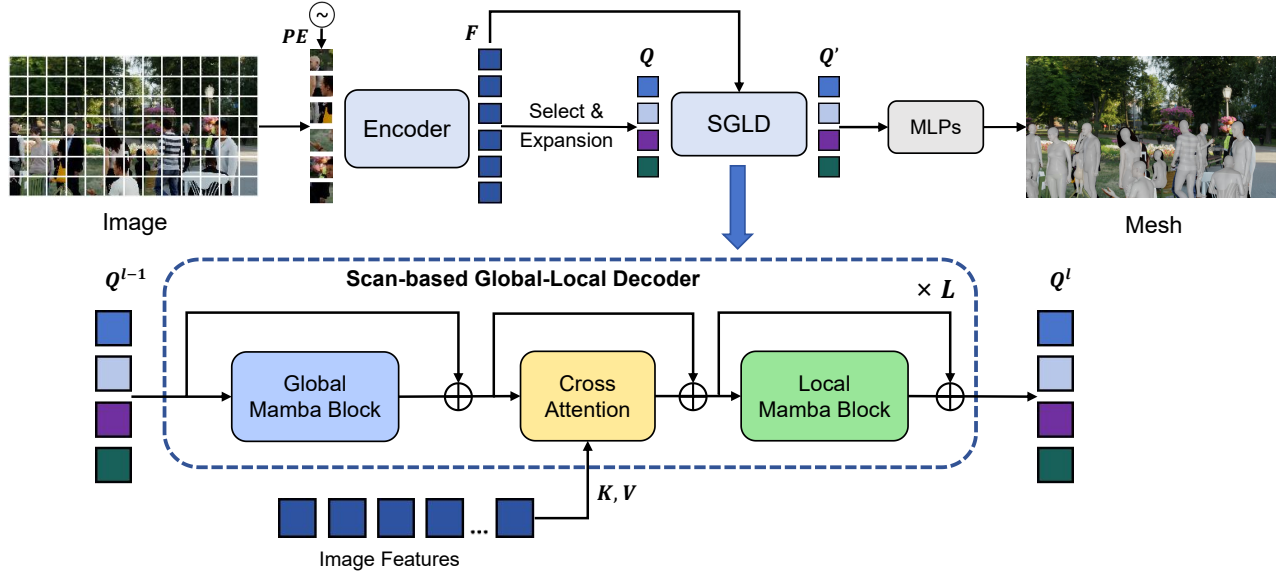


Figure 2. **Overview of the proposed EMO-X.** The input image is encoded into human tokens and expanded to whole-body primary joints. It is then fed into Scan-based Global-Local Decoder (SGLD) for global-to-local refinement based on different scanning mechanism, ultimately regressing the SMPL-X parameters.

mechanism [26] has contributed significantly to the success of these methods. However, due to its quadratic computational complexity, computational demands increase substantially with the number of tokens, especially in the multi-person setting. This results in reduced inference efficiency, requiring a trade-off between accuracy and computational efficiency.

2.2. State Space Models

State Space Models (SSMs) have gained increasing attention in recent years. They utilize recurrent scanning to store contextual information in their hidden states and update the output by combining these states with the input. Structured State Space Models (S4) [38] enhance computational efficiency through reparameterization and can model long-range dependency. Mamba [27] further improves S4 by introducing an input-dependent selection mechanism, which achieves linear time efficiency in long-sequence modeling and becomes an effective alternative to popular Transformers.

Subsequently, numerous works [28, 29, 39, 41, 61] have applied Mamba to vision tasks. Vision Mamba [28] introduces a bidirectional SSM block for data-dependent global visual context modeling. VMamba [29] explores the cross-scan to better capture the spatial relation. PoseMamba [40] uses SSMs to 2D-to-3D lifting human pose estimation, introducing a reordering strategy to enhance local modeling capabilities. PoseMagic [61] and Hamba [41] combine Mamba with Graph Convolutional Networks (GCNs) [45, 52] to capture the semantic and spatial relationships be-

tween keypoints. Our method is similar to them in applying the SSM architecture, but we introduce a novel whole-body Local Bidirectional Scan mechanism while considering multi-person mesh recovery, which has higher requirements on global-local modeling compared to single-person tasks. We are the first to demonstrate the potential of SSMs in the multi-person EHPS task.

3. Method

3.1. Preliminaries

State Space Models. SSMs [27, 38] define a continuous system that maps input sequence $x(t) \in \mathbb{R}$ to $y(t) \in \mathbb{R}$ through the latent state $h(t) \in \mathbb{R}^N$. This process can be described by ordinary linear differential equations as follows:

$$\begin{aligned} h'(t) &= \mathbf{A}h(t) + \mathbf{B}x(t), \\ y(t) &= \mathbf{C}h(t), \end{aligned} \quad (1)$$

where $\mathbf{A} \in \mathbb{R}^{N \times N}$ and $\mathbf{B}, \mathbf{C} \in \mathbb{R}^N$ are the weighting parameters. To obtain the output sequence $y(t)$ at time t , we need to find $h(t)$ which is difficult to solve analytically. For practical computation, these continuous dynamical systems are discretized as:

$$\begin{aligned} h_t &= \bar{\mathbf{A}}h_{t-1} + \bar{\mathbf{B}}x_t, \\ y_t &= \mathbf{C}h_t, \end{aligned} \quad (2)$$

where $\bar{\mathbf{A}}$ and $\bar{\mathbf{B}}$ are the discretized state parameters, which are obtained by using the well-performed Zero-Order

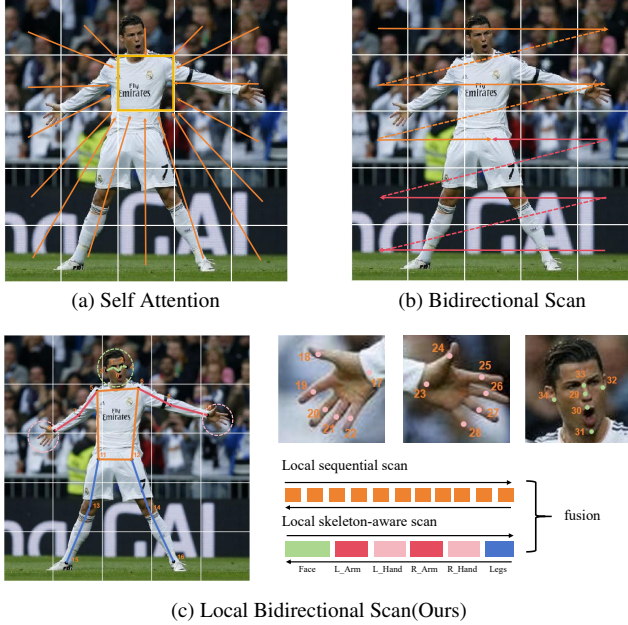


Figure 3. **Visual comparisons of different scanning mechanism.** (a) Self Attention. (b) Bidirectional Scan. (c) Our proposed Local Bidirectional Scan mechanism combines the sequential scan and the skeleton-aware scan.

Hold [42] discretization approach:

$$\bar{A} = \exp(\Delta A) \quad \bar{B} = (\Delta A)^{-1}(\exp(\Delta A) - I) \cdot \Delta B, \quad (3)$$

where Δ is the discrete step size.

However, matrices in SSMs remain unchanged regardless of the input, thus lacking content-based inference capability. In contrast, Mamba [27] expands the projection matrices to process the input sequence via a selective scan, and introduces a hardware-aware algorithm, enabling parallelization. Compared with Transformers, Mamba demonstrates high-quality and efficient modeling capability of long-range dependency.

3.2. Overview

Fig. 2 illustrates the architecture of the proposed EMO-X model. Our approach employs an Encoder-Decoder architecture, consisting of an Encoder, a Scan-based Global-Local Decoder (SGLD) and a prediction head composed of MLPs. Given an input image I , it is divided into patches of size $P \times P$. These patches are then transformed into token representations through patch embedding and position embedding, and refined by a pretrained encoder to obtain extracted image features F .

To improve computational efficiency, we select a subset of tokens from F based on classification scores to obtain body tokens T , which represent global features and location information for each human body. We then utilize T

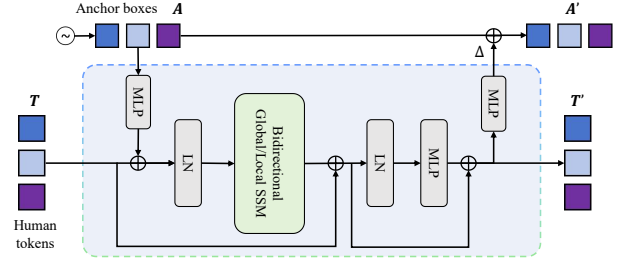


Figure 4. **Illustration of Bidirectional Mamba Block.** We employ the same structure for both Global and Local Mamba Block. The difference is the scanning mechanism and the dimension of the input tokens.

to initialize the corresponding anchor boxes A through an MLP. Next, we expand the selected tokens to obtain whole-body primary joint tokens, denoted as human queries Q . The definition of joint tokens follows AiOS [24], which represents a set of body, face and hands tokens. We refine the queries through L layers of the SGLD. Throughout the refinement process, the continuously updated anchor boxes A and the image features F serve as guidance. The outputs of each module are regressed through corresponding MLPs to predict class, bounding box, joint locations, and SMPL-X parameters, based on their respective semantics. We apply supervision to these predictions.

Loss. The overall loss functions is the sum of all the losses across each stage, encompassing the classification loss \mathcal{L}_{cls} , bounding box loss \mathcal{L}_{box} , joint location loss \mathcal{L}_{j2d} , and the SMPL-X loss \mathcal{L}_{smplx} , which includes the parameter loss \mathcal{L}_{param} , 3d keypoint loss \mathcal{L}_{kp3d} , and the 2d keypoint reprojection loss \mathcal{L}_{kp2d} . Specifically, \mathcal{L}_{cls} is a focal loss [49]. \mathcal{L}_{box} contains L1 loss and the GIOU loss [48]. \mathcal{L}_{j2d} consists of the L1 loss and Object Keypoint Similarity (OKS) loss [47]. \mathcal{L}_{param} , \mathcal{L}_{kp3d} and \mathcal{L}_{kp2d} are all L1 losses.

3.3. Bidirectional Mamba Block

To achieve high-quality and efficient long-range modeling for capturing global dependencies, we designed the Bidirectional Mamba Block (Fig. 4) as the basic block and stacked it in the Scan-based Global-Local Decoder. We perform bidirectional scanning on the input token sequence for better context modeling.

For the design of the block, we partially refer to the VSS Block proposed by Vmamba [29]. For each VSS Block, Layer Normalization (LN), SSM Block, Depth-Wise Convolution (DWConv) [59] and residual connections [60] are employed. Formally, the process can be outlined as follows:

$$\begin{aligned} T_o &= \text{LN}(\text{SSM}(\sigma(\text{DW}(\text{LN}(T_{in})))))) + T_{in}, \\ T' &= \text{MLP}(\text{LN}(T_o)), \end{aligned} \quad (4)$$

where T_{in} is the input, $\sigma(\cdot)$ represents the SiLU activation function [50] and $\text{DW}(\cdot)$ means depth-wise convolution.

However, we found that directly processing the human tokens through the VSS Block leads to suboptimal detection performance. Following DAB-DETR [51], we retain the design of anchor boxes A as explicit positional priors, embedding them as positional encoding in the input. Simultaneously, we compute 4D offsets for the anchor boxes based on the continuously updated human tokens, adding them to the previous anchor boxes. The complete structure of the Bidirectional Mamba Block is illustrated in Fig. 4, and is formulated as follows:

$$\begin{aligned} T_{in} &= T + \text{MLP}(\text{PE}(A)), \\ A' &= A + \text{MLP}(T'), \end{aligned} \quad (5)$$

where $T \in \mathbb{R}^{N \times D}$ and $A \in \mathbb{R}^{N \times 4}$ are the inputs to our Mamba Block. N is the length of human tokens and D is the embedding dimension. $\text{PE}(\cdot)$ means positional encoding to generate sinusoidal embeddings. The guidance provided by learnable anchor boxes enhances the model’s spatial awareness, leading to improved robustness in multi-person tasks.

3.4. Scan-based Global-Local Decoder

As shown in Fig. 2, our Scan-based Global-Local Decoder consists of three parts: Global Mamba Block, Cross Attention, and Local Mamba Block. Global and Local Mamba Block have the same structure (Fig. 4), with the distinction being the scanning mechanism and the dimension of the input tokens, which also gives rise to the name SGLD.

Scanning Mechanism. The Transformer-based methods compute the correlations between all tokens through Self Attention, resulting in a quadratic computational complexity. This is because for each token, all other tokens must be scanned once, as illustrated in Fig. 3a. When the number of tokens becomes large, this leads to a significant computational cost.

Vision Mamba [28] first proposed a bidirectional scanning SSM block to model global context. As shown in Fig. 3b, they sequentially scanned all tokens in the forward and backward branches and merged the features obtained after passing through the SSM block. This scanning mechanism enables the model to capture bidirectional global context information while maintaining linear computational complexity.

However, our task requires greater emphasis on capturing detailed structural features of human body to achieve high-quality EHPS. From the experiments, we found that relying solely on bidirectional global scanning leads to inaccurate reconstruction results due to its limited ability to capture local information. Therefore, we introduce a novel Local Bidirectional Scan mechanism. As shown in Fig. 3c, we consider the token set for each human separately and perform skeleton-aware scanning by defining a more reasonable joint scanning sequence.

Methods	Params (M)	Time (ms)	F1-Score \uparrow	MVE \downarrow	MPJPE \downarrow
Multi-stage Methods ($N=5$)					
OSX [19]	366.6	370.0 / 734.7	0.94	122.8	119.9
SMPLer-X [17]	668.7	257.5 / 978.5	0.93	99.7	96.8
One-stage Methods					
Multi-HMR [23]	304.0	225.7	0.94	95.9	95.7
AiOS [24]		77.0	0.94	91.9	90.2
EMO-X	127.7	124.8	0.92	91.9	90.5

Table 1. **Comparison of Efficiency.** We compare our model parameters (M), inference time (ms), F1-Score, MVE (mm) and MPJPE (mm) with the Transformer-based methods on AGORA. The number of individuals (N) in the test cases is set to 5. For multi-stage methods, we report the inference time with and without the detector separately. **Red:** Best. **Blue:** Second best.

In this mechanism, the local sequential scan performs bidirectional sequential scanning on the primary joint tokens we defined, while the local skeleton-aware scan follows a specific joint topology order for bidirectional scanning to enhance the modeling of human structural details. Our Local Bidirectional Scan mechanism integrates these two scanning sequences and processes them together through the SSM block.

Scan-based Global-Local Decoder. The SGLD takes the whole-body primary joint token queries $Q \in \mathbb{R}^{B \times M \times D}$ as input, where B represents batch size, $M = N \times J$ is the length of human tokens, N is the number of selected human and J is the number of defined primary joints. We utilize MLP to obtain corresponding anchor boxes $A \in \mathbb{R}^{B \times M \times 4}$.

First, all human tokens are refined through the Global Mamba Block, employing the Bidirectional Scan mechanism to perform global context modeling and information fusion, while perceiving the interactions between individuals. This results in the token sequence $Q_G \in \mathbb{R}^{B \times M \times D}$. In order to better utilize the image features and background information, we then use Q_G as the query and the image feature F as the key-value for cross attention to obtain the refined token sequence $Q_C \in \mathbb{R}^{B \times M \times D}$. This process associates the human token with the corresponding position in the image.

Finally, we rearrange the human token into $Q_L \in \mathbb{R}^{(B \times N) \times J \times D}$, considering each individual independently to pass through the Local Mamba Block. Here, the proposed Local Bidirectional Scan mechanism is employed to perform skeleton-aware refinement to enhance local details. After rearranging the output, we obtain the final output of this SGLD layer, denoted as $Q' \in \mathbb{R}^{B \times M \times D}$, which also serves as input for the next layer. Throughout the process, anchor boxes A serve as positional priors and are continuously updated.

Methods	F-Score \uparrow	Precision \uparrow	Recall \uparrow	NMVE \downarrow		NMJE \downarrow		MVE \downarrow					MPJPE \downarrow				
				All	Body	All	Body	All	Body	Face	LHand	RHand	All	Body	Face	LHand	RHand
BEDLAM [34]	0.73	0.98	0.59	179.5	132.2	177.5	131.4	131.0	96.5	25.8	38.8	39.0	129.6	95.9	27.8	36.6	36.7
H4W [14] \dagger	0.94	0.96	0.92	144.1	96.0	141.1	92.7	135.5	90.2	41.6	46.3	48.1	132.6	87.1	46.1	44.3	46.2
OSX [19] \dagger	0.94	0.96	0.93	130.6	85.3	127.6	83.3	122.8	80.2	36.2	45.4	46.1	119.9	78.3	37.9	43.0	43.9
HybriK-X [54]	0.93	0.95	0.92	120.5	73.7	115.7	72.3	112.1	68.5	37.0	46.7	47.0	107.6	67.2	38.5	41.2	41.4
SMPLer-X [17]	0.93	0.96	0.90	133.1	88.1	128.9	84.6	123.8	81.9	37.4	43.6	44.8	119.9	78.7	39.5	41.4	44.8
SMPLer-X [17] \dagger	0.93	0.96	0.90	107.2	68.3	104.1	66.3	99.7	63.5	29.9	39.1	39.5	96.8	61.7	31.4	36.7	37.2
Multi-HMR [23]	0.94	0.96	0.92	102.0	63.4	101.8	64.1	95.9	59.6	27.7	40.2	40.9	95.7	60.3	29.2	38.1	39.0
AiOS [24]	0.94	0.98	0.90	97.8	61.3	96.0	60.7	91.9	57.6	24.6	38.7	39.6	90.2	57.1	25.7	36.4	37.3
EMO-X	0.92	0.98	0.87	99.9	63.3	98.4	62.9	91.9	58.2	24.2	38.1	38.9	90.5	57.9	25.1	35.9	36.8

Table 2. **AGORA testing set.** \dagger denotes the methods are fine-tuned on the AGORA training set. **Red:** Best. **Blue:** Second best.

4. Experiment

4.1. Experimental Setup

Due to the page limit, we leave the detailed experiment setup, implementation, partial qualitative comparison with the state-of-the-art (SOTA) methods, and more benchmark results and analyses in the Supplementary Material.

Datasets. We use AGORA[33], BEDLAM[34], COCO [53] and single-person datasets UBody [19] as the training set, and evaluating our model on AGORA, EHF[1], UBody and BEDLAM.

Implementation. EMO-X is implemented in Pytorch and trained with AdamW [43] optimizer using a learning rate of $1e-4$ on 4 NVIDIA GeForce RTX 4090 GPUs.

Evaluation metrics. Following the previous EHPS methods [14, 17, 19, 24], we report Procrustes Aligned per-vertex position error (PA-MPVPE) and the mean per-vertex position error (MPVPE) across all benchmarks. In AGORA Leaderboard, we report mean vertex error (MVE), mean per-joint position error (MPJPE) for pure reconstruction accuracy. Detection accuracy is measured by using F-score, precision, and recall. Normalized mean vertex error (NMVE) and normalized mean joint error (NMJE) are used to consider regression accuracy with detection accuracy. All reported metrics are in millimeters (mm). To evaluate model efficiency, the number of model parameters (Params) and inference time (ms) on an NVIDIA GeForce RTX 4090 GPU are given.

4.2. Comparisons with SOTA

Our motivation is to improve the computational efficiency of multi-person EHPS, so we compare EMO-X with the Transformer-based methods on the AGORA testing set. The results are provided by the leaderboard¹.

Multi-stage methods typically employ a pre-trained detector to first detect human boxes, and then feed the cropped images into the main model. The specific computational cost is positively correlated with the number of people N . To ensure a relatively fair comparison between multi-stage

and one-stage methods in multi-person scenarios, we evaluate on the test sample with 5 individuals ($N=5$), and report the inference time with and without the detector for multi-stage methods. As illustrated in Table 1, our model stands out by achieving the best performance metrics in terms of inference time and Mean Vertex Error (MVE), all while maintaining competitive reconstruction accuracy. Specifically, EMO-X significantly reduces the inference time by 69.8% compared to AiOS [24], decreasing from 413.2 ms to 124.8 ms. Remarkably, it accomplishes this reduction while achieving the same MVE of 91.9 mm, highlighting the effectiveness and efficiency of our approach in processing multi-person scenarios.

As shown in Table 2, we further comprehensively compare the accuracy of our EMO-X with the SOTA methods on the AGORA testing set. To ensure a fair comparison, we employed a threshold of 0.5 to filter the detected samples with low confidence, which typically exhibit severe occlusion. As shown in Table 2, our EMO-X outperforms most existing methods in terms of NMVE and NMJE, second only to AiOS. Regarding the pure reconstruction quality, particularly for faces and hands, our EMO-X achieves the SOTA performance. This significant improvement is attributed to our novel local skeleton-aware design, which effectively refines the local details of whole-body, a critical aspect that has been overlooked by most existing approaches.

Methods	PA-PVE (mm) \downarrow			PVE (mm) \downarrow		
	All	Hands	Face	All	Hands	Face
PIXIE [13]	61.7	12.2	4.2	168.4	55.6	45.2
H4W [14]	44.8	8.9	2.8	104.1	45.7	27.0
OSX [19]	42.4	10.8	2.4	92.4	47.7	24.9
OSX [19] \dagger	42.2	8.6	2.0	81.9	41.5	21.2
SMPLer-X [17]	33.2	10.6	2.8	61.5	43.3	23.1
SMPLer-X [17] \dagger	31.9	10.3	2.8	57.4	40.2	21.6
Multi-HMR [23]	21.0	7.2	1.8	51.2	25.0	16.2
AiOS [24]	32.5	7.3	2.8	58.6	39.0	19.6
EMO-X	27.6	7.3	2.5	51.1	33.2	19.2

Table 3. **UBody testing set.** \dagger denotes the methods are fine-tuned on the UBody training set. **Red:** Best. **Blue:** Second best.

¹<https://agora-evaluation.is.tuebingen.mpg.de/>



Figure 5. **Qualitative results on AGORA.** Red circles highlight the areas where the estimations are inaccurate.

Methods	PA-PVE↓ (mm)			PVE↓ (mm)		
	All	Hands	Face	All	Hands	Face
H4W [14]	50.3	10.8	5.8	76.8	39.8	26.1
OSX [19]	48.7	15.9	6.0	70.8	53.7	26.4
SMPLer-X [17]	37.8	15.0	5.1	65.4	49.4	17.4
Multi-HMR [23]	28.2	10.8	5.3	42.0	28.9	18.0
AiOS [24]	34.0	12.8	3.8	45.4	44.1	16.9
EMO-X	34.7	11.7	4.4	45.3	39.5	17.1

Table 4. **EHF testing set.** **Red:** Best. **Blue:** Second best.

Besides, we also conduct a comparison with SOTA methods using single-person real datasets, UBody and EHF. See Table 3 and Table 4 for details. Our method also demonstrates superior performance compared to most existing approaches. Notably, the EHF dataset was not included in our training set, which demonstrates the generalization ability of our model.

In addition, we perform a qualitative comparison with SOTA methods [17, 23, 24]. As shown in Fig. 5, 6, the visualization results on AGORA and in-the-wild images are presented, respectively. Importantly, our method achieves excellent reconstruction quality across different scenarios, particularly in details of hands and faces.

4.3. Ablation Study

We analyze the effectiveness of the proposed components in detail. All experiments are trained only on the AGORA [33] training set and evaluated on its validation set.

Bidirectional Mamba Block. To validate the positional prior effect of anchor boxes in our Bidirectional Mamba Block, we conducted ablation experiments on it. As shown in the upper part of Table 5, when only human tokens are processed through the VSS Block, the reconstruction performance is poor. This is because the model currently con-

Settings	PA-PVE↓ (mm)			PVE↓ (mm)		
	All	Hands	Face	All	Hands	Face
Bidirectional Mamba Block						
w/o Anchor boxes	40.5	7.4	4.0	53.7	38.6	23.8
Ours	39.3	7.2	3.8	51.1	37.2	22.8
Scan-based Global-Local Decoder						
MLPs only	51.2	9.3	4.8	89.6	52.8	41.3
G only	42.6	8.6	4.3	56.6	42.8	28.8
L only	42.1	8.7	4.2	59.2	43.4	28.9
G + CA	40.1	7.4	4.0	51.8	38.6	23.8
G + L	41.7	7.6	4.0	54.7	39.6	25.7
CA + L	40.8	7.6	4.1	52.8	38.9	24.5
G + CA + L (Ours)	39.3	7.2	3.8	51.1	37.2	22.8

Table 5. **Ablation study of the Scan-based Global-Local Decoder.** G, CA, and L represent Global Mamba Block, Cross-Attention, and Local Mamba Block, respectively. All models are trained on the AGORA dataset.

Settings	PA-PVE↓ (mm)			PVE↓ (mm)		
	All	Hands	Face	All	Hands	Face
Unidirectional Scan	40.9	7.6	4.2	52.4	39.0	24.2
Bidirectional Scan	40.3	7.3	4.2	51.9	38.0	23.8
Local Unidirectional Scan	39.7	7.2	4.0	51.8	37.4	23.3
Local Bidirectional Scan (Ours)	39.3	7.2	3.8	51.1	37.2	22.8

Table 6. **Ablation study of the scan mechanism.** All models are trained on the AGORA dataset.

siders the selected human tokens in isolation, neglecting global information and positional priors. After introducing the guidance of anchor boxes, PA-PVE and PVE were reduced by 1.2 mm and 2.6 mm, respectively.

Scan-based Global-Local Decoder. We validate the impact of different components of our Scan-based Global-Local Decoder. We replace all components with simple

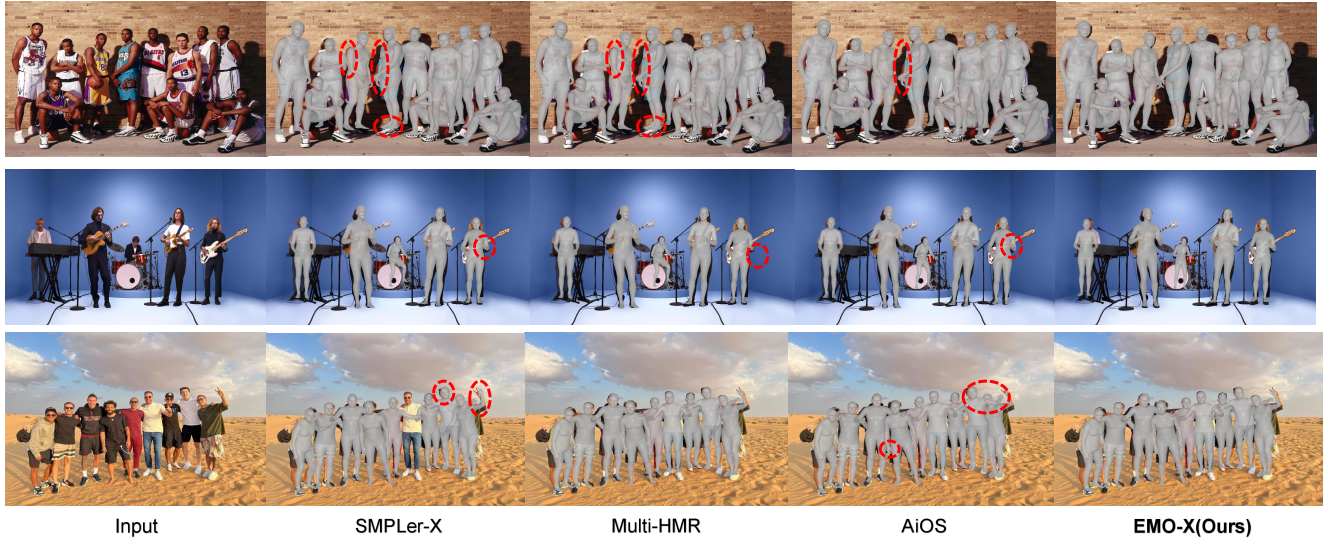


Figure 6. **Qualitative results on the in-the-wild images.** Red circles highlight the areas where the estimations are inaccurate.

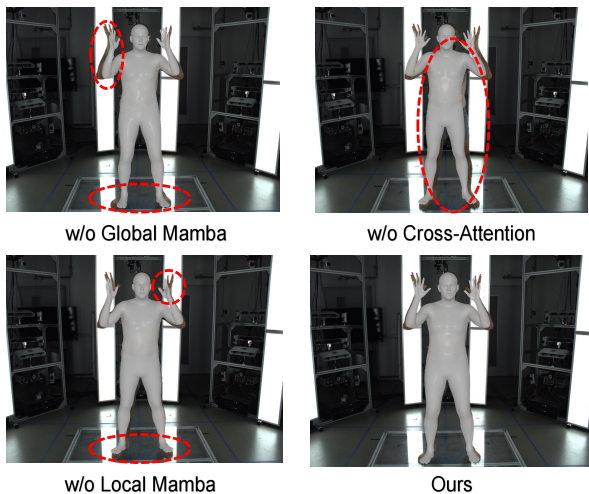


Figure 7. **Qualitative Ablation of the Scan-based Global-Local Decoder.** Our experiments are conducted on EHF. Red circles highlight the areas where the estimations are inaccurate.

MLPs as the baseline. The results are shown in Table 5. It can be seen that different components contribute to improving the accuracy of our method.

To delve deeper into the specific functions of each component, we conduct a qualitative analysis using the EHF dataset, as illustrated in Fig. 7. This allows us to visually assess the effectiveness of the individual components in action. From our comparison, it becomes clear that the Global Mamba Block and Cross-Attention have the greatest impact on the overall position. This is because Global Mamba Block models global context and the Cross-Attention asso-

ciates human tokens with the positional information contained in image features. When the Local Mamba Block is removed, there are some flaws in local details. This is because Local Mamba Block supplements local details based on whole-body topology.

Scanning Mechanism. We conducted further ablation experiments on the proposed scanning mechanism. As shown in the table 6, compared with the common bidirectional scan, modeling human tokens using unidirectional scan resulted in an increase of 0.6 mm and 0.5 mm in PA-PVE and PVE, respectively. The proposed Local Bidirectional Scan further reduced PA-PVE by 1.0 mm and PVE by 0.8 mm. This demonstrates the improved ability of our proposed scanning mechanism to capture local details.

5. Conclusion

In this work, we propose a efficient novel one-stage expressive human pose and shape estimation (EHPS) method, EMO-X, to address the trade-off between accuracy and efficiency. Specifically, we present a Scan-based Global-Local Decoder (SGLD) to progressively refine human tokens by comprehensively considering global context and local details. Notably, we incorporate a novel Local Bidirectional Scan mechanism for skeleton-aware refinement. Extensive experiments have demonstrated that our EMO-X method achieves significantly efficiency improvement (69.8% inference time decrease) meanwhile obtains satisfactory accuracy. We hope that our work can offer a new perspective for the field.

Limitations. Our EMO-X method does not explicitly consider the human-human interaction, thus is not general enough for severe occlusion and interaction scenarios.

References

- [1] G. Pavlakos, V. Choutas, N. Ghorbani, T. Bolkart, A. A. Osman, D. Tzionas, and M. J. Black, “Expressive body capture: 3d hands, face, and body from a single image,” in *Proceedings of the IEEE/CVF conference on computer vision and pattern recognition*, 2019, pp. 10975–10985. 1, 2, 6
- [2] A. Kanazawa, M. J. Black, D. W. Jacobs, and J. Malik, “End-to-end recovery of human shape and pose,” in *Proceedings of the IEEE conference on computer vision and pattern recognition*, 2018, pp. 7122–7131. 1
- [3] M. Kocabas, C.-H. P. Huang, O. Hilliges, and M. J. Black, “Pare: Part attention regressor for 3d human body estimation,” in *Proceedings of the IEEE/CVF international conference on computer vision*, 2021, pp. 11 127–11 137.
- [4] N. Kolotouros, G. Pavlakos, M. J. Black, and K. Daniilidis, “Learning to reconstruct 3d human pose and shape via model-fitting in the loop,” in *Proceedings of the IEEE/CVF international conference on computer vision*, 2019, pp. 2252–2261.
- [5] J. Li, C. Xu, Z. Chen, S. Bian, L. Yang, and C. Lu, “Hybrik: A hybrid analytical-neural inverse kinematics solution for 3d human pose and shape estimation,” in *Proceedings of the IEEE/CVF conference on computer vision and pattern recognition*, 2021, pp. 3383–3393.
- [6] Z. Li, J. Liu, Z. Zhang, S. Xu, and Y. Yan, “Cliff: Carrying location information in full frames into human pose and shape estimation,” in *European Conference on Computer Vision*. Springer, 2022, pp. 590–606.
- [7] W. Wang, Y. Ge, H. Mei, Z. Cai, Q. Sun, Y. Wang, C. Shen, L. Yang, and T. Komura, “Zolly: Zoom focal length correctly for perspective-distorted human mesh reconstruction,” in *Proceedings of the IEEE/CVF International Conference on Computer Vision*, 2023, pp. 3925–3935.
- [8] H. Zhang, Y. Tian, X. Zhou, W. Ouyang, Y. Liu, L. Wang, and Z. Sun, “Pymaf: 3d human pose and shape regression with pyramidal mesh alignment feedback loop,” in *Proceedings of the IEEE/CVF international conference on computer vision*, 2021, pp. 11 446–11 456.
- [9] Y. Deng, J. Yang, S. Xu, D. Chen, Y. Jia, and X. Tong, “Accurate 3d face reconstruction with weakly-supervised learning: From single image to image set,” in *Proceedings of the IEEE/CVF conference on computer vision and pattern recognition workshops*, 2019, pp. 0–0.
- [10] A. Tewari, M. Zollhofer, H. Kim, P. Garrido, F. Bernard, P. Perez, and C. Theobalt, “Mofa: Model-based deep convolutional face autoencoder for unsupervised monocular reconstruction,” in *Proceedings of the IEEE international conference on computer vision workshops*, 2017, pp. 1274–1283. 1
- [11] A. Boukhayma, R. d. Bem, and P. H. Torr, “3d hand shape and pose from images in the wild,” in *Proceedings of the IEEE/CVF conference on computer vision and pattern recognition*, 2019, pp. 10 843–10 852.
- [12] T. Chatzis, A. Stergioulas, D. Konstantinidis, K. Dimitropoulos, and P. Daras, “A comprehensive study on deep learning-based 3d hand pose estimation methods,” *Applied Sciences*, vol. 10, no. 19, p. 6850, 2020. 1
- [13] Y. Feng, V. Choutas, T. Bolkart, D. Tzionas, and M. J. Black, “Collaborative regression of expressive bodies using moderation,” in *2021 International Conference on 3D Vision (3DV)*. IEEE, 2021, pp. 792–804. 1, 2, 6
- [14] G. Moon, H. Choi, and K. M. Lee, “Accurate 3d hand pose estimation for whole-body 3d human mesh estimation,” in *Proceedings of the IEEE/CVF Conference on Computer Vision and Pattern Recognition*, 2022, pp. 2308–2317. 6, 7
- [15] V. Choutas, G. Pavlakos, T. Bolkart, D. Tzionas, and M. J. Black, “Monocular expressive body regression through body-driven attention,” in *Computer Vision—ECCV 2020: 16th European Conference, Glasgow, UK, August 23–28, 2020, Proceedings, Part X 16*. Springer, 2020, pp. 20–40. 2
- [16] H. Zhang, Y. Tian, Y. Zhang, M. Li, L. An, Z. Sun, and Y. Liu, “Pymaf-x: Towards well-aligned full-body model regression from monocular images,” *IEEE Transactions on Pattern Analysis and Machine Intelligence*, vol. 45, no. 10, pp. 12 287–12 303, 2023. 1, 2
- [17] Z. Cai, W. Yin, A. Zeng, C. Wei, Q. Sun, W. Yanjun, H. E. Pang, H. Mei, M. Zhang, L. Zhang *et al.*, “Smpler-x: Scaling up expressive human pose and shape estimation,” *Advances in Neural Information Processing Systems*, vol. 36, 2024. 1, 2, 5, 6, 7
- [18] H. E. Pang, Z. Cai, L. Yang, Q. Tao, Z. Wu, T. Zhang, and Z. Liu, “Towards robust and expressive whole-body human pose and shape estimation,” *Advances in Neural Information Processing Systems*, vol. 36, 2024. 1, 2
- [19] J. Lin, A. Zeng, H. Wang, L. Zhang, and Y. Li, “One-stage 3d whole-body mesh recovery with component aware transformer,” in *Proceedings of the IEEE/CVF Conference on Computer Vision and Pattern Recognition*, 2023, pp. 21 159–21 168. 1, 2, 5, 6, 7
- [20] Y. Sun, Q. Bao, W. Liu, Y. Fu, M. J. Black, and T. Mei, “Monocular, one-stage, regression of multiple 3d people,” in *Proceedings of the IEEE/CVF international conference on computer vision*, 2021, pp. 11 179–11 188. 2
- [21] Y. Sun, Q. Bao, W. Liu, T. Mei, and M. J. Black, “Trace: 5d temporal regression of avatars with dynamic cameras in 3d environments,” in *Proceedings of the IEEE/CVF Conference on Computer Vision and Pattern Recognition*, 2023, pp. 8856–8866.
- [22] Y. Sun, W. Liu, Q. Bao, Y. Fu, T. Mei, and M. J. Black, “Putting people in their place: Monocular regression of 3d people in depth,” in *Proceedings of the IEEE/CVF Conference on Computer Vision and Pattern Recognition*, 2022, pp. 13 243–13 252.
- [23] F. Baradel, M. Armando, S. Galaoui, R. Brégier, P. Weinzaepfel, G. Rogez, and T. Lucas, “Multi-hmr: Multi-person whole-body human mesh recovery in a single shot,” *arXiv preprint arXiv:2402.14654*, 2024. 2, 5, 6, 7
- [24] Q. Sun, Y. Wang, A. Zeng, W. Yin, C. Wei, W. Wang, H. Mei, C.-S. Leung, Z. Liu, L. Yang *et al.*, “Aios: All-in-one-stage expressive human pose and shape estimation,” in *Proceedings of the IEEE/CVF Conference on Computer Vision and Pattern Recognition*, 2024, pp. 1834–1843. 2, 4, 5, 6, 7
- [25] N. Carion, F. Massa, G. Synnaeve, N. Usunier, A. Kirillov, and S. Zagoruyko, “End-to-end object detection with

- transformers,” in *European conference on computer vision*. Springer, 2020, pp. 213–229. 2
- [26] A. Vaswani, “Attention is all you need,” *Advances in Neural Information Processing Systems*, 2017. 2, 3
- [27] A. Gu and T. Dao, “Mamba: Linear-time sequence modeling with selective state spaces,” *arXiv preprint arXiv:2312.00752*, 2023. 2, 3, 4
- [28] L. Zhu, B. Liao, Q. Zhang, X. Wang, W. Liu, and X. Wang, “Vision mamba: Efficient visual representation learning with bidirectional state space model,” *arXiv preprint arXiv:2401.09417*, 2024. 2, 3, 5
- [29] Y. Liu, Y. Tian, Y. Zhao, H. Yu, L. Xie, Y. Wang, Q. Ye, and Y. Liu, “Vmamba: Visual state space model,” *arXiv preprint arXiv:2401.10166*, 2024. 2, 3, 4
- [30] M. Loper, N. Mahmood, J. Romero, G. Pons-Moll, and M. J. Black, “SMPL: A skinned multi-person linear model,” *ACM Trans. Graphics (Proc. SIGGRAPH Asia)*, vol. 34, no. 6, pp. 248:1–248:16, Oct. 2015. 2
- [31] J. Romero, D. Tzionas, and M. J. Black, “Embodied hands: Modeling and capturing hands and bodies together,” *ACM Transactions on Graphics, (Proc. SIGGRAPH Asia)*, vol. 36, no. 6, Nov. 2017.
- [32] T. Li, T. Bolkart, M. J. Black, H. Li, and J. Romero, “Learning a model of facial shape and expression from 4d scans,” *ACM Trans. Graph.*, vol. 36, no. 6, pp. 194–1, 2017. 2
- [33] P. Patel, C.-H. P. Huang, J. Tesch, D. T. Hoffmann, S. Tripathi, and M. J. Black, “Agora: Avatars in geography optimized for regression analysis,” in *Proceedings of the IEEE/CVF Conference on Computer Vision and Pattern Recognition*, 2021, pp. 13 468–13 478. 2, 6, 7
- [34] M. J. Black, P. Patel, J. Tesch, and J. Yang, “Bedlam: A synthetic dataset of bodies exhibiting detailed lifelike animated motion,” in *Proceedings of the IEEE/CVF Conference on Computer Vision and Pattern Recognition*, 2023, pp. 8726–8737. 2, 6
- [35] Z. Cai, D. Ren, A. Zeng, Z. Lin, T. Yu, W. Wang, X. Fan, Y. Gao, Y. Yu, L. Pan *et al.*, “Humman: Multi-modal 4d human dataset for versatile sensing and modeling,” in *European Conference on Computer Vision*. Springer, 2022, pp. 557–577.
- [36] Z. Cai, M. Zhang, J. Ren, C. Wei, D. Ren, Z. Lin, H. Zhao, L. Yang, C. C. Loy, and Z. Liu, “Playing for 3d human recovery,” *arXiv preprint arXiv:2110.07588*, 2021.
- [37] Z. Yang, Z. Cai, H. Mei, S. Liu, Z. Chen, W. Xiao, Y. Wei, Z. Qing, C. Wei, B. Dai *et al.*, “Synbody: Synthetic dataset with layered human models for 3d human perception and modeling,” in *Proceedings of the IEEE/CVF International Conference on Computer Vision*, 2023, pp. 20 282–20 292. 2
- [38] A. Gu, K. Goel, and C. Ré, “Efficiently modeling long sequences with structured state spaces,” *arXiv preprint arXiv:2111.00396*, 2021. 3
- [39] T. Huang, X. Pei, S. You, F. Wang, C. Qian, and C. Xu, “Localmamba: Visual state space model with windowed selective scan,” *arXiv preprint arXiv:2403.09338*, 2024. 3
- [40] Y. Huang, J. Liu, K. Xian, and R. C. Qiu, “Posemamba: Monocular 3d human pose estimation with bidirectional global-local spatio-temporal state space model,” 2024. [Online]. Available: <https://arxiv.org/abs/2408.03540> 3
- [41] H. Dong, A. Chharia, W. Gou, F. V. Carrasco, and F. D. la Torre, “Hamba: Single-view 3d hand reconstruction with graph-guided bi-scanning mamba,” 2024. [Online]. Available: <https://arxiv.org/abs/2407.09646> 3
- [42] A. Iserles, *A first course in the numerical analysis of differential equations*. Cambridge university press, 2009, no. 44. 4
- [43] I. Loshchilov, “Decoupled weight decay regularization,” *arXiv preprint arXiv:1711.05101*, 2017. 6
- [44] J. Yang, A. Zeng, S. Liu, F. Li, R. Zhang, and L. Zhang, “Explicit box detection unifies end-to-end multi-person pose estimation,” in *International Conference on Learning Representations*, 2023. [Online]. Available: <https://openreview.net/forum?id=s4WVupnJjmX> 2
- [45] T. N. Kipf and M. Welling, “Semi-supervised classification with graph convolutional networks,” *arXiv preprint arXiv:1609.02907*, 2016. 3
- [46] J. B. Lee, R. A. Rossi, X. Kong, S. Kim, E. Koh, and A. Rao, “Higher-order graph convolutional networks,” *arXiv preprint arXiv:1809.07697*, 2018.
- [47] D. Shi, X. Wei, L. Li, Y. Ren, and W. Tan, “End-to-end multi-person pose estimation with transformers,” in *Proceedings of the IEEE/CVF Conference on Computer Vision and Pattern Recognition*, 2022, pp. 11 069–11 078. 4
- [48] H. Rezatofighi, N. Tsoi, J. Gwak, A. Sadeghian, I. Reid, and S. Savarese, “Generalized intersection over union: A metric and a loss for bounding box regression,” in *Proceedings of the IEEE/CVF conference on computer vision and pattern recognition*, 2019, pp. 658–666. 4
- [49] T. Lin, “Focal loss for dense object detection,” *arXiv preprint arXiv:1708.02002*, 2017. 4
- [50] F. Wang, J. Cheng, W. Liu, and H. Liu, “Additive margin softmax for face verification,” *IEEE Signal Processing Letters*, vol. 25, no. 7, pp. 926–930, 2018. 4
- [51] S. Liu, F. Li, H. Zhang, X. Yang, X. Qi, H. Su, J. Zhu, and L. Zhang, “Dab-detr: Dynamic anchor boxes are better queries for detr,” *arXiv preprint arXiv:2201.12329*, 2022. 2, 5
- [52] L. Zhao, X. Peng, Y. Tian, M. Kapadia, and D. N. Metaxas, “Semantic graph convolutional networks for 3d human pose regression,” in *Proceedings of the IEEE/CVF conference on computer vision and pattern recognition*, 2019, pp. 3425–3435. 3
- [53] T.-Y. Lin, M. Maire, S. Belongie, J. Hays, P. Perona, D. Ramanan, P. Dollár, and C. L. Zitnick, “Microsoft coco: Common objects in context,” in *Computer Vision—ECCV 2014: 13th European Conference, Zurich, Switzerland, September 6–12, 2014, Proceedings, Part V 13*. Springer, 2014, pp. 740–755. 6
- [54] J. Li, S. Bian, C. Xu, Z. Chen, L. Yang, and C. Lu, “Hybrikx: Hybrid analytical-neural inverse kinematics for whole-body mesh recovery,” *arXiv preprint arXiv:2304.05690*, 2023. 6
- [55] G. Moon, H. Choi, and K. M. Lee, “Neuralannot: Neural annotator for 3d human mesh training sets,” in *Proceedings of the IEEE/CVF Conference on Computer Vision and Pattern Recognition*, 2022, pp. 2299–2307.

- [56] M. Contributors, “Openmmlab 3d human parametric model toolbox and benchmark,” 2021.
- [57] W. Liu, D. Anguelov, D. Erhan, C. Szegedy, S. Reed, C.-Y. Fu, and A. C. Berg, “Ssd: Single shot multibox detector,” in *Computer Vision–ECCV 2016: 14th European Conference, Amsterdam, The Netherlands, October 11–14, 2016, Proceedings, Part I 14*. Springer, 2016, pp. 21–37. [1](#)
- [58] J. Redmon, S. Divvala, R. Girshick, and A. Farhadi, “You only look once: Unified, real-time object detection,” in *Proceedings of the IEEE conference on computer vision and pattern recognition*, 2016, pp. 779–788. [1](#)
- [59] F. Chollet, “Xception: Deep learning with depthwise separable convolutions,” in *Proceedings of the IEEE conference on computer vision and pattern recognition*, 2017, pp. 1251–1258. [4](#)
- [60] K. He, X. Zhang, S. Ren, and J. Sun, “Deep residual learning for image recognition,” in *Proceedings of the IEEE conference on computer vision and pattern recognition*, 2016, pp. 770–778. [4](#)
- [61] X. Zhang, Q. Bao, Q. Cui, W. Yang, and Q. Liao, “Pose magic: Efficient and temporally consistent human pose estimation with a hybrid mamba-gcn network,” *CoRR*, 2024. [3](#)
- [62] M. Oquab, T. Darcet, T. Moutakanni, H. Vo, M. Szafraniec, V. Khalidov, P. Fernandez, D. Haziza, F. Massa, A. El-Nouby *et al.*, “Dinov2: Learning robust visual features without supervision,” *arXiv preprint arXiv:2304.07193*, 2023.